

ARTICLE OPEN

Similar spatial patterns of global climate response to aerosols from different regions

Matthew Kasoar^{1,2}, Dilshad Shawki^{1,2} and Apostolos Voulgarakis¹

Anthropogenic aerosol forcing is spatially heterogeneous, mostly localised around industrialised regions like North America, Europe, East and South Asia. Emission reductions in each of these regions will force the climate in different locations, which could have diverse impacts on regional and global climate. Here, we show that removing sulphur dioxide (SO₂) emissions from any of these northern-hemisphere regions in a global composition-climate model results in significant warming across the hemisphere, regardless of the emission region. Although the temperature response to these regionally localised forcings varies considerably in magnitude depending on the emission region, it shows a preferred spatial pattern independent of the location of the forcing. Using empirical orthogonal function analysis, we show that the structure of the response is tied to existing modes of internal climate variability in the model. This has implications for assessing impacts of emission reduction policies, and our understanding of how climate responds to heterogeneous forcings.

npj Climate and Atmospheric Science (2018)1:12; doi:10.1038/s41612-018-0022-z

INTRODUCTION

Anthropogenic aerosols are a significant driver of the climate system,¹ and are particularly interesting to study as climate forcers because of their short lifetimes. This means that their radiative forcing is very inhomogeneous, possibly affecting the climate differently depending on the source region. It also means that policy decisions have the potential to change aerosol forcing very quickly. A large number of previous studies have provided valuable insight into the impacts that historical aerosol changes have had on the climate,^{2–7} but for evaluating policy choices it would also be useful to understand the separate contributions of different regions, because future emission changes are unlikely to mirror historical trajectories everywhere. Such a regional breakdown could also be more informative for understanding the behaviour of the climate system when driven by localised forcings, allowing the effect of historical emissions from different locations to be disentangled.

So far though, very few studies have attempted to systematically investigate the sensitivity of the climate to different forcing distributions. Important work pursued by one modelling group in recent years has investigated climate responses to forcing within different latitude bands^{8,9}; however, anthropogenic aerosol emissions are far from zonally uniform within the northern hemisphere—there is large inhomogeneity in the zonal direction as well. In particular, the major industrialised regions of North America, Europe, and East Asia all lie within the northern mid-latitudes. It is therefore pressing to understand how the sensitivity of the climate might depend on the longitudinal as well as latitudinal location of an aerosol forcing, by investigating geographically more localised regions rather than latitude bands or historical northern hemisphere changes.

Apart from the physical insight, such a breakdown of climate response by region driving it has the potential to be more

informative for policy applications, since emission reduction policies are determined regionally, and not harmonised across the hemisphere or indeed within a particular latitude band. Policy measures also cannot directly scale atmospheric forcing or concentration distributions, but instead can target only the actual emissions from that region, and so investigating responses as a function of realistic regional emissions has again the potential to be more directly applicable than some previous regional studies, in which atmospheric concentrations were scaled.^{8–10}

RESULTS

Modelling of regional aerosol emission reductions

To address this, we have performed a series of composition-climate model simulations (see Methods) to investigate how the global climate responds to localised sulphate precursor emissions from different parts of the world. Recent multi-model studies^{11,12} have indicated that, at recent emission levels, sulphate is the dominant anthropogenic aerosol contributor to climate forcing over black carbon or organic carbon. We also performed simulations perturbing regional black carbon emissions but, consistent with these studies, we were unable to observe any significant large-scale climate impacts for realistic emission changes, and so results for black carbon are not presented here.

Figure 1 shows the distribution of anthropogenic sulphur dioxide emissions—the principal precursor to sulphate aerosol—circa the year 2000.¹³ As indicated by the boxes in Fig. 1, we pick out four major emission regions: North America, Europe, East Asia, and South Asia, and in addition we also consider the northern hemisphere mid-latitudes (NHML) as an entire latitude band. For each of these regions we performed a simulation where sulphur dioxide emission rates are instantaneously reduced to zero within that region alone, while being kept at year-2000 levels elsewhere.

¹Department of Physics, Imperial College London, SW7 2AZ London, UK and ²Grantham Institute—Climate Change and the Environment, Imperial College London, SW7 2AZ London, UK

Correspondence: Matthew Kasoar (m.kasoar12@imperial.ac.uk)

Received: 18 August 2017 Revised: 24 January 2018 Accepted: 30 January 2018

Published online: 21 June 2018

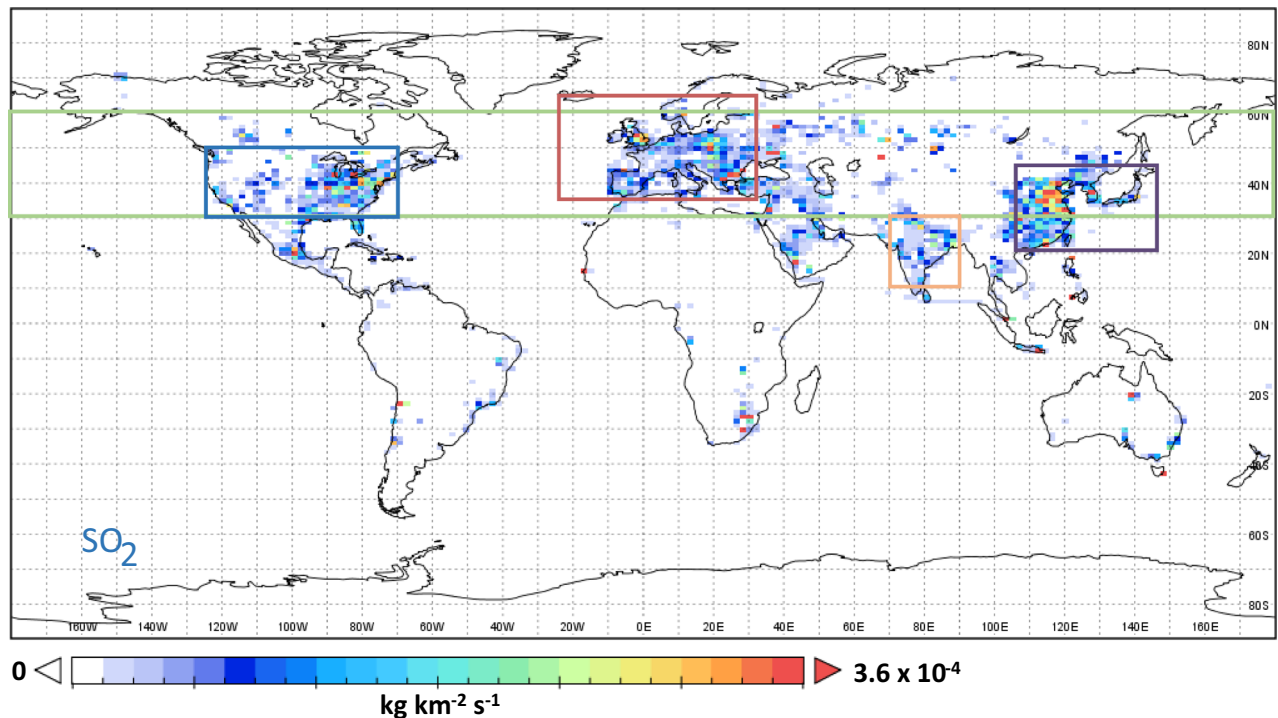


Fig. 1 Anthropogenic SO_2 emissions circa year 2000. We show the annual mean of the control SO_2 emissions used to drive our simulations, which were taken from the ACCMIP dataset.¹³ The boxes show the regions in which emissions were removed in each of the perturbation experiments: the northern mid-latitudes (NHML, green), North America (blue), Europe (red), East Asia (purple), and South Asia (orange). For Europe, the HTAP Phase II European region definition was used, which follows EU country borders on the eastern boundary, and hence the eastern edge of the box is indicative rather than exact. For the other regions emissions were removed in the latitude and longitude bounds shown, as detailed in Methods

Due to their short atmospheric lifetimes, sulphur dioxide and its oxidation product, sulphate, are not transported far from the original source region in large quantities. As a result, the radiative forcing is highly inhomogeneous, and in each case localised around the region where emissions are reduced (Fig. 2). Previous studies by the Hemispheric Transport of Air Pollution (HTAP) project^{14,15} have also investigated the importance of transport for regional aerosol forcing, and found similarly that for sulphate, the dominant forcing contribution generally remains close to the source region. Sulphate aerosol strongly scatters incoming solar radiation, and so its removal in our experiments results here in a positive radiative heating mainly over the perturbed region.

Global mean responses to different regional forcings

We diagnose the climate responses due to these aerosol forcings from fully coupled atmosphere-ocean simulations, averaged over 150 simulation years to isolate the signal from internal variability. The global mean changes in SO_2 emissions, effective radiative forcing (ERF), and the global surface temperature and precipitation responses, are summarised in Table 1. We note that the climate model used here also produced the strongest response to sulphate aerosol changes out of nine models that participated in the recent Precipitation Driver and Response Model Intercomparison Project,¹⁶ and so the magnitude of the responses seen here is likely an upper bound. However, our focus here is more on the relative changes and pattern of response from different regions.

Global temperature and precipitation changes are significant in all experiments, although only very marginally so for the South Asian emissions perturbation, which is also the perturbation featuring by far the smallest emissions change. Sulphate aerosol has minimal atmospheric absorption, and so, as expected from theoretical arguments and from other modelling studies,^{16–18} global mean precipitation change appears to scale closely with

global mean surface temperature change. The ratio of total precipitation change to temperature change is consistently around $0.07\text{--}0.08 \text{ mm day}^{-1} \text{ K}^{-1}$ for all SO_2 perturbations. This equates to around $2.2\text{--}2.5\% \text{ K}^{-1}$, and agrees very well with the hydrological sensitivities to global temperature changes that have been established in previous multi-model studies,^{16,17} and in particular falls within the range of the “slow” precipitation responses identified as being due to long-term, ocean-mediated temperature change in Table 2 of ref. ¹⁸, which reported $2.1\text{--}3.1\% \text{ K}^{-1}$.

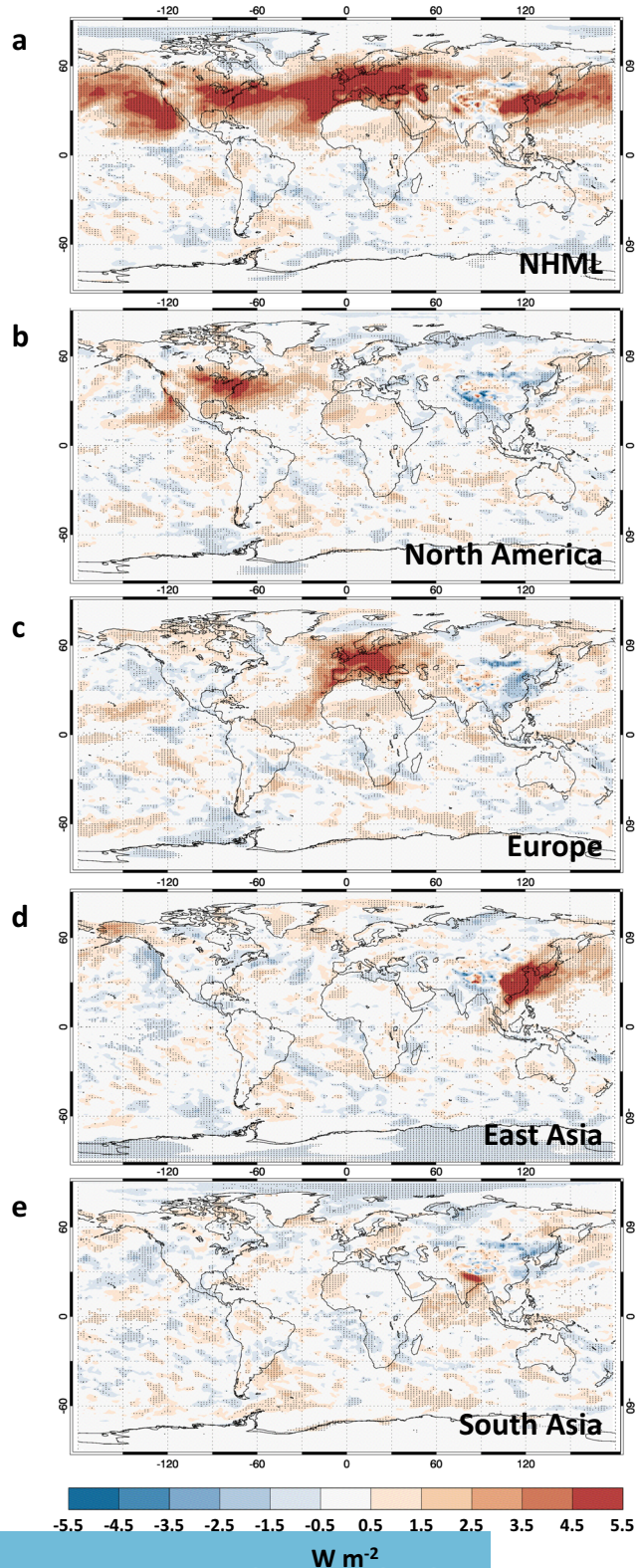
The magnitudes of the global changes vary considerably with region—of particular note is the comparison between the SO_2 removals from North America, Europe, and East Asia. Removing East Asian SO_2 emissions corresponds to a substantially larger emissions reduction than either the North America or Europe emissions perturbations—a 20% reduction in global emissions compared with 14 or 15% reductions. Despite this, the global radiative forcing, temperature and precipitation changes are all significantly larger in the cases of North American or European emission perturbations. This is also consistent with the stronger response per unit SO_2 emission from Europe compared with East Asia reported in a previous multi-model study,^{19,20} which diagnosed radiative forcings and estimated global temperature change metrics from a range of emission species in these two regions.

Strikingly, when normalised by the change in SO_2 emissions (Supplementary Table 1), the NHML forcing per unit emission change turns out to be almost exactly the arithmetic mean of the forcing per unit emissions change for the North America, Europe, and East Asia perturbations—the three regions which combined make up most of the NHML emissions—in spite of the differences in forcing per unit emission among these regions.

We attribute this large variation in the forcing per unit emission change from different regions to the role of clouds and indirect

aerosol effects. Focusing on the shortwave component (Supplementary Table S2), the clear-sky forcing—due only to the aerosol direct effect—is modest in all cases, and indeed is slightly larger for the East Asia SO₂ removal than for the North America or Europe perturbations, consistent with the larger change in aerosol burden in the East Asia case. However, the all-sky shortwave forcing, which includes interactions with clouds, is much greater

Fig. 2 Effective radiative forcing (ERF) due to removing SO₂ emissions from **a** the northern hemisphere mid-latitudes (NHML), **b** North America, **c** Europe, **d** East Asia, and **e** South Asia. The annual mean ERF is diagnosed from atmosphere-only simulations with prescribed sea-surface temperatures, as the difference in the net top-of-atmosphere radiative flux between the perturbation simulations and a control simulation, averaged over 25 years. Stippling indicates that the ERF value at that grid-point exceeded 2 standard deviations of the control simulation's annual mean top-of-atmosphere radiative flux, as described in the Methods section



than the clear-sky forcing in all experiments, but ranges from roughly doubling (in the East Asia experiment) to more than quadrupling (in the South Asia experiment) the clear-sky shortwave forcing.

The indirect radiative forcing due to the inclusion of clouds therefore makes a very substantial difference to the final forcing of the climate system, but it also makes a more substantial difference to the North America and Europe forcings than to the East Asia forcing, with the North America and Europe all-sky shortwave forcings being greater than their respective clear-sky shortwave forcings by a much larger factor. This could be explained by a saturation of aerosol–cloud interactions over East Asia, as well as greater climatological cloud cover masking the direct aerosol forcing over East Asia, as described also in the additional discussion accompanying Supplementary Tables 1 and 2.

Between the North America, Europe, and East Asia SO₂ reductions, it is the European emissions change that produces the largest radiative forcing. However, it is the North American perturbation that stimulates the largest global temperature response, indicating that the response per unit global forcing, or climate sensitivity, may also vary depending on the location of a given regional forcing (see the Supplementary Information for further discussion).

Spatial patterns of the climate response

The global mean responses provide useful metrics, but of greater relevance to many stakeholders will be the regional climate impacts. Given that the applied forcings are geographically quite localised, we might expect large regional responses that depart from the global mean changes, depending on the location of the emission perturbation. Supplementary Fig. 1 shows the geographic surface temperature response in each experiment, but in Fig. 3a–e we show the surface temperature responses with the global mean temperature change subtracted off, to highlight the regional patterns of the response. Interestingly, we find that warming is consistently seen in locations right across the northern hemisphere, often far from the location of the forcing, though strongly confined to the same hemisphere. This creates a considerable hemispheric asymmetry in warming (Supplementary Table 3) which accounts for much of the geographic precipitation response (Supplementary Fig. 2), which is dominated by northward shifts in tropical precipitation across all ocean basins. Although ubiquitous, the temperature responses are not zonally uniform within the northern hemisphere, however. The temperature responses do indeed show a distinct regionality, particularly across the mid-latitudes, with areas of substantially greater or less warming than the global mean. However, this regionality in the response also seems to be very consistent between perturbations, with a striking similarity in the spatial pattern of response between the different experiments evident in Fig. 3.

The local region where each emission perturbation was applied does consistently experience the largest mid-latitude temperature changes, but all the SO₂ removal experiments additionally show a distinctive common pattern of mid-latitude temperature

Table 1. Global mean climate responses

	Δ SO ₂ emissions (Tg yr ⁻¹)	ERF (W m ⁻²)	Δ Temperature (K)	Δ Precipitation (mm day ⁻¹)
NHML	-64.0 (-61.7%)	0.906 ± 0.052	0.821 ± 0.052	0.0624 ± 0.0040
North America	-14.2 (-13.7%)	0.232 ± 0.052	0.233 ± 0.052	0.0174 ± 0.0040
Europe	-15.0 (-14.5%)	0.275 ± 0.052	0.195 ± 0.052	0.0159 ± 0.0040
East Asia	-20.6 (-19.9%)	0.166 ± 0.052	0.119 ± 0.052	0.0080 ± 0.0040
South Asia	-5.5 (-5.3%)	0.101 ± 0.052	0.060 ± 0.052	0.0041 ± 0.0040

We calculate the global changes in emissions, top-of-atmosphere effective radiative forcing (ERF), surface temperature, and total precipitation, due to removing anthropogenic SO₂ emissions from the northern mid-latitudes (NHML), North America, Europe, East Asia, and South Asia, in HadGEM3-GA4. Surface temperature and precipitation changes are diagnosed from 150-year annual averages of coupled simulations, while ERF is diagnosed from 25-year annual averages of atmosphere-only simulations. Annual mean emissions changes are given both as an absolute value and as a percentage reduction relative to total global emissions. Error ranges for ERF, temperature, and precipitation changes due to internal variability are taken as 2 standard deviations of the respective variable in the control simulations, as described in Methods

anomalies, with elevated warming over North America and a “tongue” of warming extending into the western Atlantic (blue box, Fig. 3a–e), elevated warming over parts of central Russia (yellow box, Fig. 3a–e), and, in the NHML, North America, and East Asia perturbations, a tongue of warming extending from Japan into the western Pacific (green box, Fig. 3a, b, d). This is in addition to very consistent stronger warming across the Arctic region in all experiments, this region being known to be especially sensitive due to a number of positive temperature feedbacks.^{21–24}

Comparing with the surface temperature responses seen in experiments with more homogenous forcings like doubling CO₂ or increasing the solar constant (Supplementary Fig. 3), many features of the northern hemisphere response are similar. As well as the Arctic amplification of the response, much of the warming pattern over the North Atlantic and Eurasia, including elevated warming over parts of central Russia, are common features regardless of the forcing mechanism in this model. However, some details of the response to the regional aerosol forcings are distinct, such as the pattern of warming over central North America which occurs in all the regional aerosol perturbations but not in response to global forcings (compare Fig. 3a–e and Supplementary Fig. 1 with Supplementary Fig. 3). The regional aerosol perturbations are more similar to each other in their mid-latitude responses than they are to CO₂ or solar forcing responses, in addition to the hemispheric asymmetry in the temperature response, indicating there is still sensitivity to the latitudinal structure of the forcing.

These similar spatial patterns of stronger northern mid-latitude response are not restricted just to the surface temperature, but are also found in associated dynamical responses. For instance, the change in 500 hPa geopotential height (Fig. 3f–j), which is a measure of pressure anomalies in the mid-troposphere, again shows a remarkably similar spatial pattern of changes in the northern hemisphere in each of the SO₂ emissions removal experiments. In particular, they all show a very similar positive geopotential height anomaly over eastern North America and the west Atlantic, associated with the blue box in Fig. 3a–e, and almost all also show a distinct positive anomaly over central or northern Russia, associated with the yellow box in Fig. 3a–e.

DISCUSSION

Empirical orthogonal function (EOF) analysis of modes of internal variability

To investigate further why the temperature and dynamical changes so consistently follow these patterns, apparently regardless of the longitudinal position of the emissions and forcing, we compute the EOFs of annual surface temperature and geopotential height in the control simulation (see Methods). The EOFs decompose the timeseries of these variables into orthogonal

spatial patterns, the (time varying) superposition of which can reconstruct the complete 200-year timeseries of the control simulation. In principle, this can expose the leading spatial modes of variability in the climate system—or in this case the simulated climate.

The three leading modes for global surface temperature and 500 hPa geopotential height between them explain 35–40% of the total variability in the simulated climate system (Supplementary Table 4). The first mode is not particularly revealing (see Supplementary Figs. 4–6 and associated discussion in the Supplementary Information). However, the second EOF modes of both surface temperature and geopotential height are far more interesting. Ignoring the ENSO-like pattern in the Pacific, the second surface temperature EOF (Fig. 4a) is dominated by a pattern in the northern hemisphere which includes same-sign changes over North America, north-east Europe and Russia, and in the western Pacific extending out from Japan, which bear a distinct spatial resemblance to the patterns of temperature change in the three boxed regions identified in Fig. 3a–e. The second geopotential height EOF (Fig. 4b) is also dominated by an anomaly over North America and the Atlantic which is very similar to that seen in the geopotential height changes in Fig. 3f–j, although over Europe and Russia it is less similar. This US/North Atlantic pattern is also seen somewhat convolved with the third temperature and geopotential height EOFs (Supplementary Fig. 4b, d), although the third geopotential height EOF is mostly seen to pick out a Southern Annual Mode behaviour.

These patterns already existed in the control simulation, as spatial patterns of naturally occurring internal modelled climate variability. As described above, we consider that EOF 2 in Fig. 4 likely represents the actual leading pattern of intrinsic mid-latitude variability in the model climate. The second and third surface temperature EOFs in this model display an encouraging similarity with previously reported global EOFs of observed annual temperatures from 1902 to 1980,²⁵ which lends confidence that the patterns of variability identified above in this model are also present in the real world. In particular, these second EOF modes for both the surface temperature and geopotential height have a very strong resemblance to the expected Arctic Oscillation (AO) pattern, matching closely observed surface air temperature and 500 hPa geopotential height patterns regressed onto the AO index in reanalysis data.^{26–28} The model therefore correctly re-produces the known leading patterns of variability in the northern hemisphere, and we suggest that the response to regional forcing in the northern hemisphere must, at least to some extent, be projecting onto this pre-existing mode of variability in the model climate, resulting in a response that resembles one phase of this pattern of variability.

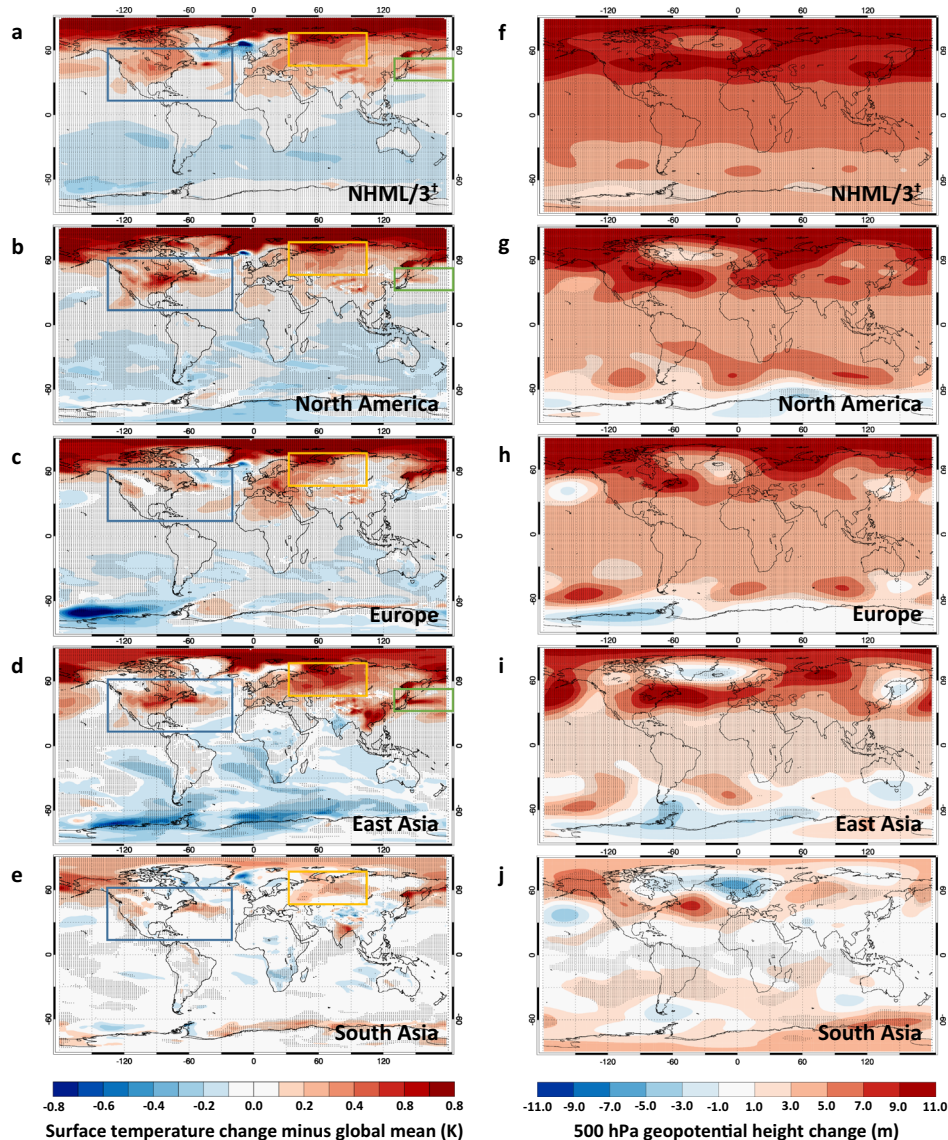


Fig. 3 Surface temperature changes minus the global mean change (a–e), and changes in 500 hPa geopotential height (f–j). a–e show the geographic pattern of 150-year annual mean surface temperature change, with the global mean temperature change subtracted off in each case, due to SO₂ emissions being removed from a, the northern mid-latitudes (NHML), b North America, c Europe, d East Asia, and e South Asia. The definition of the emission perturbation regions is as shown in Fig. 1 and described in Methods. The blue, yellow, and green rectangles highlight regions with consistent regional patterns of stronger temperature change, as discussed in the text. f–j show the corresponding 150-year annual mean changes in the 500 hPa geopotential height for each perturbation. In all plots, stippling indicates that the change at that grid-point exceeded 2 standard deviations of the 150-year mean in six different control simulations, as described in the Methods section. † Note that the NHML changes have been divided by 3 in order to show them on the same contour scale

Based on theoretical arguments and idealised dynamical core model experiments, it has been suggested in previous studies^{29,30} that regional climate responses to a forcing, being controlled strongly by atmospheric dynamics, might project onto existing modes of variability in the climate system. Notably, a projection onto the AO has previously been reported in response to historical greenhouse gas forcing in a coarse resolution climate model,²⁷ and this influence of historical climate change on modes of northern hemisphere variability has also been suggested in observations.³¹ Such a phenomenon appears to also be seen in our results, in response to localised aerosol forcing in a high-complexity global climate model. As a result, the spatial pattern of the dynamical and temperature responses is not particularly sensitive to the zonal position of the forcing (and the emission), so long as the resultant atmospheric heating is strong enough to influence the pattern of mid-latitude variability seen in the second

EOF modes in Fig. 4. We conjecture that this could potentially also explain why the North American perturbation resulted in the strongest response per unit forcing (albeit not by a statistically significant margin, see Supplementary Table S1), as the location of this forcing intersects more directly with the pattern of variability being excited over North America and the Atlantic.

Implications for policy and predictability

Our results have interesting implications for emissions mitigation policies. We have investigated the long-term climate impacts of cessation of SO₂ emissions from each of the major geographic regions that contribute to anthropogenic aerosol forcing, in a fully coupled climate model. Unsurprisingly, this unmasks a significant degree of warming globally, but also with pronounced regional variations. We find that the emission region does always

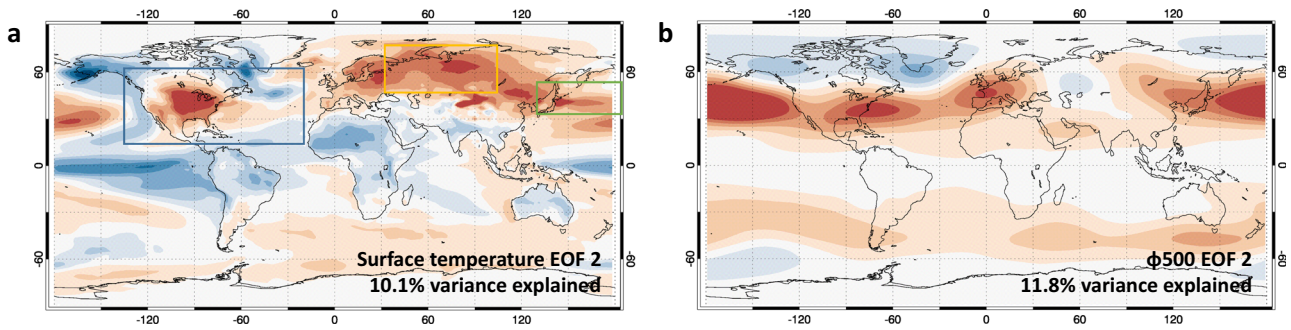


Fig. 4 Second EOF modes of global annual mean surface temperature (**a**), and 500 hPa geopotential height (ϕ 500, **b**) in the control simulation. These patterns represent the second highest contribution to the total variance in annual mean surface temperature and geopotential height over the 200 years of the model control simulation. The sign and absolute magnitude of the EOF patterns are arbitrary, so we show them here without a scale range. We have chosen the sign of the contours such that the pattern over North America and northern Eurasia is positive (red), for easier comparison with the surface temperature and geopotential height responses in Fig. 3

experience a particularly strong local temperature impact, as does the Arctic region which proves to be highly sensitive to heating from all the northern hemisphere regions. However, the most striking feature of our results is that these regionally localised aerosol perturbations also give rise to very similar large-scale climate responses, characterised by a common spatial pattern of warming across the northern hemisphere, which in turn also drives very consistent tropical precipitation changes. An important message is that even for short-lived forcing agents, the impact on climate may extend very far from the source; however, these remote effects vary strongly in space.

Still, we have demonstrated that this inhomogeneous pattern can be predictable: we have shown that the climate response to localised forcing may project onto existing modes of variability in our model climate. This suggests that a relatively small number of simulations could potentially constrain regional patterns of climate response to arbitrary forcings, and offers promise for the construction of simplified models that could be useful both for the theoretical representation of the emission-forcing-response chain, and for rapid policy-informing estimates of emission impacts on climate. If the inclination to a preferred pattern of response is robust, then it may imply that existing global or zonal perturbation studies could also be used to provide a first-order estimate of the pattern of response to regional short-lived emissions as well.

However, our results also demonstrated that the response per unit emission can vary strongly between regions. One interesting result is that normalised SO_2 emissions from North America or Europe may have a larger global (but not local) impact than those from East Asia. These results, particularly when normalised by emission perturbation as shown in Supplementary Table 1, can form a basis for constructing simple policy tools for estimating the climate response to an arbitrary combination of emissions changes from different regions, or to compare the relative impact of emissions reductions in different parts of the world. Such work is already ongoing utilising this model dataset.

Generalisation of our results is limited by the use of a single composition-climate model, as the computational effort required for such an extensive set of simulations is substantial. The magnitude of the temperature response to a regional aerosol emissions removal of this kind has been found to vary substantially across current-generation composition-climate models,^{16,32} and the extent to which other full-complexity models will show the same projection onto internal modes is unknown. However, many features of the northern hemisphere pattern of response seen here also appear in this model's response to other forcing agents like CO_2 . It may therefore be that the pattern of response to regional aerosol perturbations is rather less model dependent than the magnitude. A hint of this was seen in a recent study of the temperature response to SO_2 reduction over China,³²

where two out of three models produced very similar patterns over Eurasia, despite simulating very different magnitudes of response per unit emission change.

Given the potential to better constrain the climate impacts of different regional emissions policies, there is now a need for modelling groups to investigate the effects of similar regional emission perturbations in multiple models in a coordinated manner. This would greatly complement the existing focus on simulating historical and future scenarios, which do not isolate the contributions of individual geopolitical regions.

METHODS

We performed global, coupled atmosphere-ocean simulations with the HadGEM3-GA4 composition-climate model developed by the Met Office. The atmospheric component of the model is run with a 1.875° longitude \times 1.25° latitude horizontal resolution, and 85 vertical levels with the model top at 85 km, and is described and evaluated in ref. ³³. The ocean component of the model³⁴ has a 1° horizontal resolution, and 75 depth levels. Aerosols are simulated interactively by the CLASSIC aerosol scheme,³⁵ but with oxidant fields prescribed following ref. ³⁶. Greenhouse gases concentrations, and emissions of aerosols and aerosol precursors, are prescribed to year 2000 values based on refs. ^{13,37} throughout the simulations.

We performed six 200-year control simulations, identical except for different atmospheric initialisation states, which were used to estimate the internal variability of the model. We also performed five perturbation simulations, in each of which anthropogenic emissions of SO_2 are set to zero in one of five different regions: the northern mid-latitude band ("NHML", 30°N – 60°N), North America (235°E – 290°E , 30°N – 50°N), Europe (defined using the HTAP Phase II definition,³⁸ following country borders), East Asia (105°E – 145°E , 20°N – 45°N), and South Asia (70°E – 90°E , 10°N – 30°N). (For the North American perturbation, SO_2 emissions were removed from emission sectors as in ref. ³², corresponding to a near complete (97%) removal rather than a complete zeroing of emissions.) We focused on perturbations to sulphur dioxide, the main precursor to sulphate aerosol, as this has been shown in recent multi-model studies to give the largest present-day aerosol forcing.^{11,16} We did also investigate perturbations to black carbon emissions, but these resulted in largely insignificant large-scale surface temperature responses for realistic (100%) perturbations, similar to the results of ref. ¹¹.

For each simulation, the first 50 years of data were discarded to allow the responses to establish themselves, and the means over the remaining 150 years were analysed. Climate responses (temperature, precipitation, and geopotential height changes) were calculated by differencing the 150-year annual mean of each perturbation simulation with the 150-year mean of a single control simulation (the same control simulation was used in all cases). Uncertainty due to internal variability was estimated for each climate variable by finding the standard deviation, σ_c , among the six different control simulations' 150-year means, both at each gridpoint and for area-weighted global means. Responses in the perturbed simulations were considered significant if they differed by more than $2\sigma_c$ from the control simulation. This is equivalent to assigning a standard error of $\sqrt{2}\sigma_c$

(~84% confidence interval) to both the control and perturbation simulation values, such that the standard error in the difference is then $2\sigma_c$.

In addition to the coupled atmosphere-ocean simulations, we also performed 26-year atmosphere-only simulations with an identical model setup for control and perturbation simulations, except that sea-surface temperatures and sea-ice cover were prescribed to observed year 2000 values, repeated every year. The first year of data was discarded as spin-up. These simulations were then used to calculate ERF, as the difference between the 25-year mean top-of-atmosphere (TOA) radiative flux in each perturbation simulation, and the control simulation. Only a single control simulation was performed for the atmosphere-only case. The uncertainty in the TOA radiative flux was therefore estimated as the standard deviation of the annual mean fluxes for the 25 individual years of the control run, divided by $\sqrt{25}$, to give an estimate of the standard deviation in the 25-year mean TOA radiative flux. ERF values were again taken to be significant if they exceeded 2 standard deviations of the control simulation's mean TOA radiative flux.

EOFs of global surface temperature and 500 hPa geopotential height were calculated from the full 200-year annual mean timeseries at each gridpoint from a single coupled control simulation. The choice of control simulation analyzed was found not to qualitatively affect the EOF patterns produced, i.e., all control simulations featured similar spatial modes of variability.

Data and code availability

We encourage further uses for the data generated by the regional perturbation simulations used in this study. Archived simulation output as well as the post-processed data used for figures in this study is available from the corresponding author on reasonable request.

Use of the HadGEM3-GA4 climate model was provided by the Met Office through the Joint Weather and Climate Research Programme, and the model source code is not generally available. For more information on accessing the model, see <http://www.metoffice.gov.uk/research/collaboration/um-collaboration>.

ACKNOWLEDGEMENTS

Simulations with HadGEM3-GA4 were performed using the MONSooN system, a collaborative facility supplied under the Joint Weather and Climate Research Programme, which is a strategic partnership between the Met Office and the Natural Environment Research Council. M.K. and A.V. are supported by the Natural Environment Research Council under grant NE/K500872/1. D.S. is supported by the Grantham Institute for Climate Change and the Environment.

AUTHOR CONTRIBUTIONS

A.V. and M.K. designed the experiments. M.K. and D.S. performed the simulations. M.K. carried out the analysis and wrote the text. All authors contributed to the discussion of the results.

ADDITIONAL INFORMATION

Supplementary Information accompanies the paper on the *npj Climate and Atmospheric Science* website (<https://doi.org/10.1038/s41612-018-0022-z>).

Competing interests: The authors declare no competing interests.

Publisher's note: Springer Nature remains neutral with regard to jurisdictional claims in published maps and institutional affiliations.

REFERENCES

1. Myhre, G. et al. in *Climate Change 2013: The Physical Science Basis. Contribution of Working Group I to the Fifth Assessment Report of the Intergovernmental Panel on Climate Change* (eds Stocker, T. F. et al.) Ch. 8 (Cambridge University Press, Cambridge, United Kingdom and New York, NY, USA, 2013).
2. Bollasina, M. A., Ming, Y. & Ramaswamy, V. Anthropogenic aerosols and the weakening of the South Asian summer monsoon. *Science* **334**, 502–505 (2011).
3. Polson, D., Bollasina, M., Hegerl, G. C. & Wilcox, L. J. Decreased monsoon precipitation in the northern hemisphere due to anthropogenic aerosols. *Geophys. Res. Lett.* **41**, 6023–6029 (2014).
4. Kawase, H., Takemura, T. & Nozawa, T. Impact of carbonaceous aerosols on precipitation in tropical Africa during the austral summer in the twentieth century. *J. Geophys. Res.* **116**. <https://doi.org/10.1029/2011jd015933> (2011).
5. Hwang, Y.-T., Frierson, D. M. W. & Kang, S. M. Anthropogenic sulfate aerosol and the southward shift of tropical precipitation in the late 20th century. *Geophys. Res. Lett.* **40**, 2845–2850 (2013).
6. Wilcox, L. J., Highwood, E. J. & Dunstone, N. J. The influence of anthropogenic aerosol on multi-decadal variations of historical global climate. *Environ. Res. Lett.* **8**, 024033 (2013).
7. Booth, B. B., Dunstone, N. J., Halloran, P. R., Andrews, T. & Bellouin, N. Aerosols implicated as a prime driver of twentieth-century North Atlantic climate variability. *Nature* **484**, 228–232 (2012).
8. Shindell, D. & Faluvegi, G. Climate response to regional radiative forcing during the twentieth century. *Nat. Geosci.* **2**, 294–300 (2009).
9. Shindell, D. T., Voulgarakis, A., Faluvegi, G. & Milly, G. Precipitation response to regional radiative forcing. *Atmos. Chem. Phys.* **12**, 6969–6982 (2012).
10. Teng, H., Washington, W. M., Branstator, G., Meehl, G. A. & Lamarque, J.-F. Potential impacts of Asian carbon aerosols on future US warming. *Geophys. Res. Lett.* **39**. <https://doi.org/10.1029/2012gl015723> (2012).
11. Baker, L. H. et al. Climate responses to anthropogenic emissions of short-lived climate pollutants. *Atmos. Chem. Phys.* **15**, 8201–8216 (2015).
12. Myhre, G. et al. Radiative forcing of the direct aerosol effect from AeroCom phase II simulations. *Atmos. Chem. Phys.* **13**, 1853–1877 (2013).
13. Lamarque, J. F. et al. Historical (1850–2000) gridded anthropogenic and biomass burning emissions of reactive gases and aerosols: methodology and application. *Atmos. Chem. Phys.* **10**, 7017–7039 (2010).
14. Stjern, C. W. et al. Global and regional radiative forcing from 20% reductions in BC, OC and SO₄—an HTAP2 multi-model study. *Atmos. Chem. Phys.* **16**, 13579–13599 (2016).
15. Yu, H. et al. A multimodel assessment of the influence of regional anthropogenic emission reductions on aerosol direct radiative forcing and the role of inter-continental transport. *J. Geophys. Res. Atmos.* **118**, 700–720 (2013).
16. Samset, B. H. et al. Fast and slow precipitation responses to individual climate forcers: a PDRMIP multimodel study. *Geophys. Res. Lett.* **43**, 2782–2791 (2016).
17. Held, I. M. & Soden, B. J. Robust responses of the hydrological cycle to global warming. *J. Clim.* **19**, 5686–5699 (2006).
18. Andrews, T., Forster, P. M., Boucher, O., Bellouin, N. & Jones, A. Precipitation, radiative forcing and global temperature change. *Geophys. Res. Lett.* **37**. <https://doi.org/10.1029/2010gl043991> (2010).
19. Bellouin, N. et al. Regional and seasonal radiative forcing by perturbations to aerosol and ozone precursor emissions. *Atmos. Chem. Phys.* **16**, 13885–13910 (2016).
20. Aamaas, B., Berntsen, T. K., Fuglestad, J. S., Shine, K. P. & Bellouin, N. Regional emission metrics for short-lived climate forcers from multiple models. *Atmos. Chem. Phys.* **16**, 7451–7468 (2016).
21. Graverson, R. G. & Wang, M. Polar amplification in a coupled climate model with locked albedo. *Clim. Dyn.* **33**, 629–643 (2009).
22. Screen, J. A. & Simmonds, I. The central role of diminishing sea ice in recent Arctic temperature amplification. *Nature* **464**, 1334–1337 (2010).
23. Pithan, F. & Mauritsen, T. Arctic amplification dominated by temperature feedbacks in contemporary climate models. *Nat. Geosci.* **7**, 181–184 (2014).
24. Curry, J. A., Schramm, J. L. & Ebert, E. E. Sea ice-albedo climate feedback mechanism. *J. Clim.* **8**, 240–247 (1995).
25. Mann, M. E., Bradley, R. S. & Hughes, M. K. Global-scale temperature patterns and climate forcing over the past six centuries. *Nature* **392**, 779–787 (1998).
26. Thompson, D. W. J. & Wallace, J. M. The Arctic oscillation signature in the wintertime geopotential height and temperature fields. *Geophys. Res. Lett.* **25**, 1297–1300 (1998).
27. Shindell, D. T., Miller, R. L., Schmidt, G. A. & Pandolfo, L. Simulation of recent northern winter climate trends by greenhouse-gas forcing. *Nature* **399**, 452 (1999).
28. Rauthe, M. & Paeth, H. Relative importance of northern hemisphere circulation modes in predicting regional climate change. *J. Clim.* **17**, 4180–4189 (2004).
29. Shepherd, T. G. Atmospheric circulation as a source of uncertainty in climate change projections. *Nat. Geosci.* **7**, 703–708 (2014).
30. Ring, M. J. & Plumb, R. A. The response of a simplified GCM to axisymmetric forcings: applicability of the fluctuation–dissipation theorem. *J. Atmos. Sci.* **65**, 3880–3898 (2008).
31. Corti, S., Molteni, F. & Palmer, T. N. Signature of recent climate change in frequencies of natural atmospheric circulation regimes. *Nature* **398**, 799–802 (1999).
32. Kasoar, M. et al. Regional and global temperature response to anthropogenic SO₂ emissions from China in three climate models. *Atmos. Chem. Phys.* **16**, 9785–9804 (2016).
33. Walters, D. N. et al. The met office unified model Global Atmosphere 4.0 and JULES Global Land 4.0 configurations. *Geosci. Model Dev.* **7**, 361–386 (2014).
34. Madec, G. *NEMO Ocean Engine, No. 27. Report No. ISSN No. 1288–1619* (Institut Pierre-Simon Laplace (IPSL), France, 2008).

35. Bellouin, N. et al. Aerosol forcing in the Climate Model Intercomparison Project (CMIP5) simulations by HadGEM2-ES and the role of ammonium nitrate. *J. Geophys. Res.* **116**. <https://doi.org/10.1029/2011jd016074> (2011).
36. Derwent, R., Collins, W., Jenkin, M., Johnson, C. & Stevenson, D. The global distribution of secondary particulate matter in a 3-D Lagrangian chemistry transport model. *J. Atmos. Chem.* **44**, 57–95 (2003).
37. Meinshausen, M. et al. The RCP greenhouse gas concentrations and their extensions from 1765 to 2300. *Clim. Change* **109**, 213–241 (2011).
38. Dentener, F., Keating, T. & Guizzardi, D. Common set of source and receptor regions. <http://iek8wikis.iek.fz-juelich.de/HTAPWiki/WP2.1> (2014).



Open Access This article is licensed under a Creative Commons Attribution 4.0 International License, which permits use, sharing,

adaptation, distribution and reproduction in any medium or format, as long as you give appropriate credit to the original author(s) and the source, provide a link to the Creative Commons license, and indicate if changes were made. The images or other third party material in this article are included in the article's Creative Commons license, unless indicated otherwise in a credit line to the material. If material is not included in the article's Creative Commons license and your intended use is not permitted by statutory regulation or exceeds the permitted use, you will need to obtain permission directly from the copyright holder. To view a copy of this license, visit <http://creativecommons.org/licenses/by/4.0/>.

© The Author(s) 2018

Reproduced with permission of copyright owner. Further reproduction prohibited without permission.